B3LYP density functional calculations on the ground-state structure, elastic properties, and compression mechanism of α-ZrW$_2$O$_8$

C. A. Figueirêdo[1] and C. A. Perottoni[1,2,*]

[1]*Departamento de Física e Química, Universidade de Caxias do Sul, 95070-560 Caxias do Sul – RS, Brazil*
[2]*Instituto de Física, Universidade Federal do Rio Grande do Sul, 91501-970 Porto Alegre – RS, Brazil*

The structure of α-ZrW$_2$O$_8$ was optimized at different pressures and its elastic constants were calculated at the B3LYP density functional level of theory. Overall, the relative stiffnesses of the atomic bonds (and linkages), ranked in terms of bond compressibilities, decrease according to the sequence W-O > Zr$\cdots$W > Zr-O. The tetrahedra around tungsten atoms are found to be much stiffer than the ZrO$_6$ octahedra. These latter are, in fact, more compressible than the α-ZrW$_2$O$_8$ unit cell. The elastic constants calculated in the athermal limit are in excellent agreement with recent experimental results obtained near 0 K. The α-ZrW$_2$O$_8$ compression mechanism around W1 and W2 atoms is quite different. While the former can be described essentially in terms of a correlated polyhedral rotation, the latter involves correlated rotation of the first coordination polyhedra and translation of WO$_4$ units downward along the $\langle 111 \rangle$ axis. These modes of deformation should bear some resemblance to the low-energy modes responsible for the negative thermal expansion in zirconium tungstate, and thus could give some insight on the microscopic mechanism behind this phenomenon.

　　　　PACS number(s): 91.60.Ed, 64.30.+t, 62.20.Dc, 65.40.De

I. INTRODUCTION

Zirconium tungstate, ZrW$_2$O$_8$, has been the subject of several recent studies whose main motivation is the isotropic negative thermal expansion (NTE) exhibited by this compound over a wide range of temperature, from 0.3 to 1050 K.[1] At room conditions, zirconium tungstate (α-ZrW$_2$O$_8$) is a cubic compound, space group $P2_13$, with a linear thermal expansion coefficient of -8.8×10^{-6} K^{-1}.[1–5] The structure of α-ZrW$_2$O$_8$ can be described as an interconnected framework of ZrO$_6$ octahedra and WO$_4$ tetrahedra, with the latter having one nonbridging (terminal) oxygen (see Fig. 1). α-ZrW$_2$O$_8$ is metastable with respect to the parent binary oxides below 1380 K, and undergoes a phase transition at pressures above 0.2 GPa to γ-ZrW$_2$O$_8$, orthorhombic, space group $P2_12_12_1$.[4,6–8] At even greater pressures, zirconium tungstate amorphizes.[9,10] The amorphous phase recrystallizes into α-ZrW$_2$O$_8$ when heated above 900 K at room pressure.[11]

The NTE of ZrW$_2$O$_8$ has been attributed to low-energy, transversal vibrational modes of the Zr-O-W linkages.[1,12] A further development of this model, which take into account the linkage between the ZrO$_6$ and WO$_4$ polyhedra, is based on the concept of rigid unit modes—RUMs, and involves the tilting of nearly rigid polyhedra, whose increase in amplitude leads to contraction on heating.[13] Evidences for this low-energy lattice dynamics have been found, among others, in inelastic neutron scattering experiments and low-temperature specific heat measurements.[14,15] This picture has been challenged recently and the exact nature of the low-energy modes responsible for NTE of α-ZrW$_2$O$_8$ remains controversial. In fact, based on XAFS analysis of α-ZrW$_2$O$_8$, Cao *et al.* have suggested that NTE in zirconium tungstate is mainly caused by vibrational modes involving the correlated motion of a WO$_4$ tetrahedron and its three nearest ZrO$_6$ units.[16,17] The model proposed by Cao *et al.* rest on the experimental observation that the Zr$\cdots$W peaks in the Fourier transform of

the α-ZrW$_2$O$_8$ XAFS spectra have a very small temperature dependence and, thus, the displacements of Zr, W, and O atoms must be correlated. This observation has led to the conclusion that the Zr-O-W linkage should be quite stiff, forming a quasirigid unit of WO$_4$ and the three nearest ZrO$_6$ octahedra (which should be stiff but not rigid). According to this model, the low-frequency optical modes that lead to NTE in α-ZrW$_2$O$_8$ involve the translation of a WO$_4$ tetrahedron along the $\langle 111 \rangle$ axis and (owing to the relatively stiff Zr-O-W linkage) a correlated motion of the three nearest
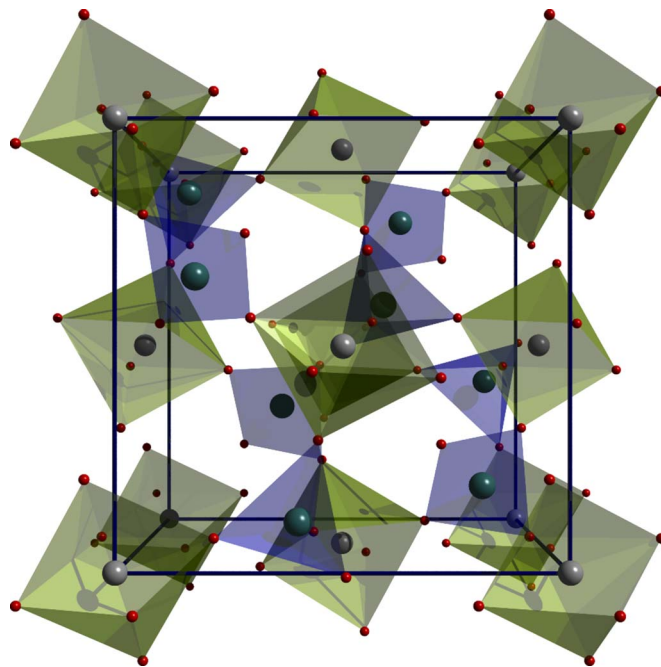

FIG. 1. (Color online) Schematic representation of the α-ZrW$_2$O$_8$ crystal structure. Green octahedra and blue tetrahedra represents the ZrO$_6$ and WO$_4$ units, respectively. This latter has a nonbridging (terminal) oxygen.

TABLE I. Zirconium basis set. Exponents (in a.u.) and coefficients of the s, p, and d Gaussian functions.

| Type | Exponent | Coefficients | | |
		s	p	d
s	3450660.8000000	0.0000340		
	467601.9400000	0.0003220		
	92314.5140000	0.0021000		
	21992.5200000	0.0112000		
	6082.9917000	0.0475000		
	1915.2715000	0.1570000		
	676.4392700	0.3524000		
	263.0026700	0.4238000		
	106.8939500	0.1593000		
sp	7730.9357000	−0.0003560	0.0009180	
	1743.6542000	−0.0065700	0.0089500	
	515.5596400	−0.0586000	0.0557000	
	176.1882400	−0.1469000	0.2190000	
	67.9467380	0.2212000	0.4536000	
	29.1731490	0.6893000	0.3970000	
	13.0012280	0.2629000	0.1064000	
sp	177.6701800	0.0039900	−0.0124000	
	59.9868760	−0.0365000	−0.0757000	
	24.1859650	−0.3385000	0.0838000	
	9.9783433	0.1865000	0.9961000	
	4.3099261	0.9971000	1.2441000	
	1.7492066	0.2468000	0.3080000	
sp	3.8653000	−1.5950000	−0.1149000	
	1.7390000	−0.3640000	0.5140000	
	0.7875000	4.9455000	1.3848000	
sp	0.3383000	1.0000000	1.0000000	
d	297.8550000			0.0059700
	87.4716000			0.0474000
	31.5134000			0.1925000
	12.3703000			0.4114000
	4.9738000			0.4381000
	1.9570000			0.1588000
d	2.6544000			0.0824000
	1.0022000			0.3192000
d	0.3493000			1.0000000

TABLE II. Oxygen basis set. Exponents (in a.u.) and coefficients of the s and p Gaussian functions.

| Type | Exponent | Coefficients | |
		s	p
s	8020.00000	0.00108	
	1338.00000	0.00804	
	255.40000	0.05324	
	69.22000	0.16810	
	23.90000	0.35810	
	9.26400	0.38550	
	3.85100	0.14680	
	1.21200	0.07280	
sp	49.43000	−0.00883	0.00958
	10.47000	−0.09150	0.06960
	3.23500	−0.04020	0.20650
	1.21700	0.37900	0.34700
sp	0.44190	1.00000	1.00000
sp	0.15750	1.00000	1.00000

The relatively narrow pressure range over which α-ZrW$_2$O$_8$ is observed experimentally makes it difficult to assert how this structure changes with pressure.[7] Computer simulations could allow us to explore the behavior of α-ZrW$_2$O$_8$ over an extended pressure range. Previous computer simulations on α-ZrW$_2$O$_8$ have been restricted to a few studies on the structure, lattice dynamics, and phase stability using interatomic potentials and, also, to a first-principles calculation mainly focused on the influence of pressure on the electronic gap.[13,20–23] In this work, the α-ZrW$_2$O$_8$ struc-

TABLE III. Tungsten valence electron basis set. Exponents (in a.u.) and coefficients of the s, p, and d Gaussian functions.

| Type | Exponent | Coefficients | | |
		s	p	d
s	14.2907290	−1.4086099		
	12.2412490	2.1936470		
	5.3122400	−1.7108013		
s	0.8718000	1.0000000		
s	0.2853000	1.0000000		
p	7.2496570		2.0610138	
	6.0848760		−3.0002471	
p	1.6904000		0.2166000	
	0.8880000		0.8069039	
p	0.3652900		1.0000000	
d	3.4651000			−0.1924000
	2.6335000			0.2055000
	0.9540000			0.4557000
	0.3756000			0.6662000
d	0.2134000			1.0000000

ZrO$_6$ octahedra (tent model). This mixed librational and translational motion in some low-energy modes of α-ZrW$_2$O$_8$ have also been inferred from the analysis of the infrared spectrum of zirconium tungstate.[18]

On the other hand, reverse Monte Carlo analysis of neutron total scattering data for α-ZrW$_2$O$_8$ led Tucker *et al.* to conclude, consistently with the rigid unit mode model, that NTE arises from RUMs involving the correlated rotation of WO$_4$ and ZrO$_6$ units.[19] Also, according to Tucker *et al.*, a rigid Zr-O-W linkage would have the effect of stiffening the structure, inhibiting NTE in zirconium tungstate.

TABLE IV. α-ZrW_2O_8 atomic positions, as optimized at the B3LYP density functional theory level, and some experimental results obtained at different temperatures. For comparison, atomic positions optimized at $P=3$ GPa (according to the EOS found in this work) are given in the last column.

Atom	Jorgensen et al. 300 K[a]	Mary et al. 293 K[b]	Evans et al. 2 K[c]	This work $a=9.3565$Å	This work $a=9.2691$Å
$x(Zr)$	0.0011	0.0003	0.0013	0.0027	0.0033
$x(W1)$	0.3401	0.3412	0.3405	0.3457	0.3446
$x(W2)$	0.6006	0.6008	0.5998	0.5969	0.5957
$x(O1)$	0.2055	0.2071	0.2063	0.2015	0.2013
$y(O1)$	0.4376	0.4378	0.4392	0.4386	0.4389
$z(O1)$	0.4467	0.4470	0.4470	0.4429	0.4433
$x(O2)$	0.7877	0.7876	0.7866	0.7827	0.7827
$y(O2)$	0.5694	0.5694	0.5676	0.5623	0.5617
$z(O2)$	0.5549	0.5565	0.5560	0.5534	0.5528
$x(O3)$	0.4922	0.4916	0.4918	0.4871	0.4852
$x(O4)$	0.2323	0.2336	0.2332	0.2375	0.2352

[a]Reference 7.
[b]Reference 1.
[c]Reference 33.

ture and elastic properties were studied according to density functional theory (DFT), aiming to explore such issues as the relative stiffness of the Zr-O-W linkage, the nature of W-O and Zr-O bonding and, also, verify to what extent computer simulations may give support to the recently observed anomalous increase of 40% in the bulk modulus of α-ZrW_2O_8 in going from 300 K to near 0 K.[24]

This paper will proceed as follows: In the next section we will present some computational details relevant to the calculations performed with α-ZrW_2O_8. In Sec. III we will present the main results obtained from the DFT calculations on α-ZrW_2O_8, concerning the structure, elastic moduli, and compression mechanism of this compound. Electronic density isosurfaces will be presented aiming to substantiate the analysis of bond compressibilities in zirconium tungstate. The paper ends with a brief discussion on the possible contribution of our results to clarify some issues related to different models for NTE in α-ZrW_2O_8.

II. COMPUTATIONAL DETAILS

All the calculations were performed in the athermal limit, with the CRYSTAL03 computer code.[25] The crystalline orbitals were each expressed as a sum of atomic-centered Gaussian functions over all equivalent sites in the periodic system. Total energies were evaluated according to the density functional theory, with the Becke's gradient-corrected hybrid exchange-correlation density functional (B3LYP).[26] All-electron basis sets were employed for both oxygen[27] and zirconium.[28] For tungsten we used the Stuttgard-Dresden energy-adjusted 14-valence electron quasirelativistic pseudopotential in combination with the corresponding valence basis sets.[29] In the calculations, valence electron f-functions and f-terms in the pseudopotential had to be omitted for tungsten. The outermost Gaussian exponents and coefficients

for the valence basis sets were optimized by minimizing the total energy for α-ZrW_2O_8. The optimized Zr and O all-electron, and W valence electron basis sets are given in Tables I, II and III, respectively. The tolerances employed in the evaluation of the infinite Coulomb and exchange series were 10^{-7} for the exchange and Coulomb overlap, Coulomb penetration, and the first exchange pseudo-overlap, and 10^{-14} for the second exchange pseudo-overlap tolerance.[25] For integrals involving effective core potentials the tolerance was 10^{-7}. The Fock matrix has been diagonalized at 45 k-points within the irreducible Brillouin zone, corresponding to a shrinkage factor of 8 in the Monkhorst net.[30] The number of k-points in the Gilat net was set to 249, corresponding to a shrinkage factor of 16.[31] To improve convergence, a level shifting of 0.5 E_h was employed and the Fock matrix was updated with a mixing of 40% with the previous Fock matrix at each iteration of the self-consistent-field procedure. Atomic positions were optimized at fixed lattice parameters using a modified conjugate gradient algorithm.[32] Convergence was achieved when the maximum gradient, the RMS gradient, the maximum atomic displacement, and the RMS atomic displacement on all atoms become less than 0.000 090, 0.000 060, 0.000 180, and 0.000 120 a.u., respectively. To reduce the influence of numerical noise, all the calculations were performed keeping the same set of indexed bielectronic integrals selected from a reference geometry. The tolerance for energy convergence was set to 10^{-9} E_h. Three distinct deformations were applied to the cubic cell of zirconium tungstate in order to evaluate the bulk modulus (B) and two independent elastic constants (c_{11} and c_{44}). The third elastic constant (c_{12}) was obtained from B and c_{11} according to[25]

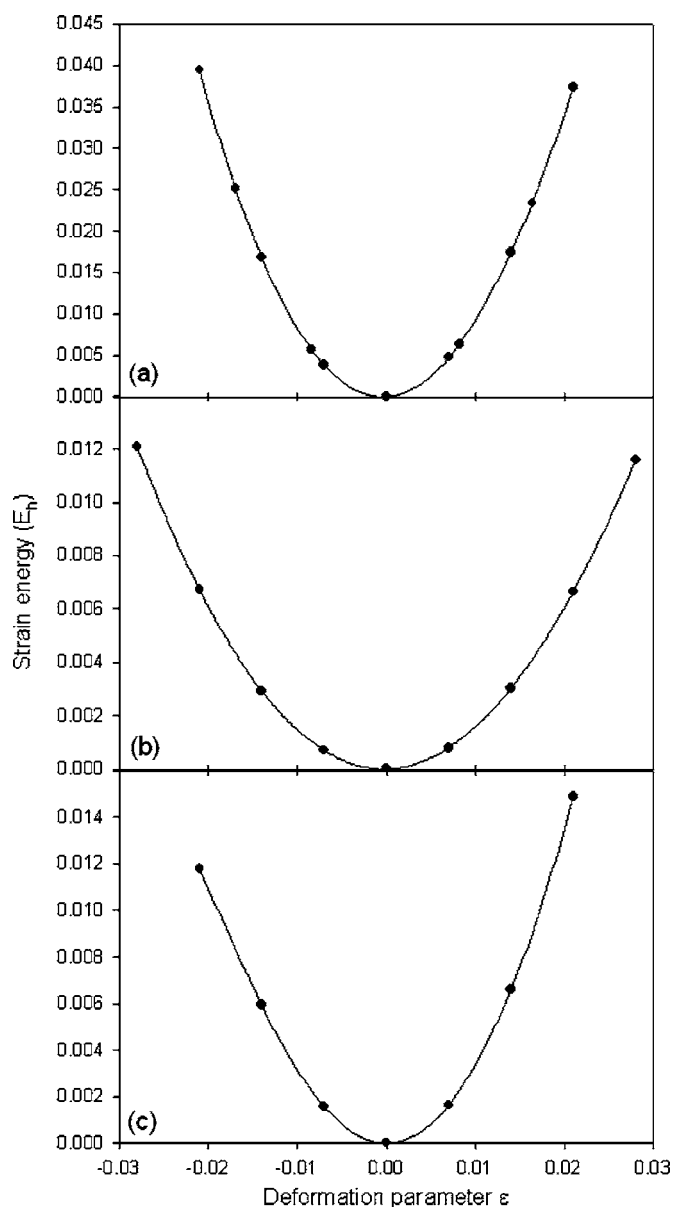$$c_{12} = \frac{3B - c_{11}}{2}. \tag{1}$$

FIG. 2. Dependence of the strain energy (in units of hartree) on the adimensional lattice deformation parameter ϵ for the calculation of the (a) bulk modulus and the elastic constants (b) c_{11} and (c) c_{44}.

Atomic positions were fully relaxed after each deformation of the unit cell. The maximum deformations were limited to $\pm 3\%$ of the equilibrium lattice parameter to reduce the influence of high-order terms in the series expansions for the strain energy. Energy second derivatives were evaluated numerically.

III. RESULTS AND DISCUSSION

The cubic phase of ZrW_2O_8 has seven independent atoms per unit cell. The full optimization of this crystal structure in the athermal limit is thus obtained by minimizing the internal energy as a function of 12 parameters (the lattice parameter plus 11 parameters for the atomic positions). The derivatives of energy with respect to lattice parameters are not imple-

TABLE V. Comparison between calculated and experimental elastic constants (c_{11}, c_{12}, and c_{44}) and bulk modulus (B), in gigapascals, at 0 K. The numbers in parentheses refer to the uncertainties from the fitting of the strain energy versus adimensional deformation curves, as depicted in Fig. 2.

Reference	c_{11}	c_{12}	c_{44}	B
Drymiotis et al.[a]	161.8	75.5	29.4	104.3
This work	161.8(1)	75.3(9)	29.6(3)	104.1(5)

[a]Reference 24.

mented in CRYSTAL03. Hence, the optimization of the α-ZrW_2O_8 crystal structure was obtained by a one-dimensional search for the equilibrium lattice parameter followed by minimization of energy with respect to atomic positions. This latter was performed using a modified conjugate gradient algorithm.[32] This two-step procedure was repeated until full convergence was achieved for all 12 parameters. The calculated lattice parameter, $a_0 = 9.3565$ Å, is about 2% greater than that obtained by Evans et al. at 2 K.[33] This slight overestimation of the lattice parameter is expected according to the general trend observed with periodic DFT calculations.[35] The atomic positions for the optimized crystal structure are given in Table IV, along with some experimental values obtained by neutron and x-ray diffraction at room temperature and near 0 K. As can be seen in Table IV, there is a good overall agreement between calculated and experimental values for the atomic positions. The main difference between calculated and experimental results is for the zirconium atomic position, which is very near the unit cell origin. However, even for the zirconium position, the distance along the $\langle 111 \rangle$ axis between the calculated position and that given by Evans et al., for instance, is only 0.02 Å or 0.2% of the lattice parameter.[4]

The three independent elastic constants (c_{11}, c_{12}, and c_{44}) of zirconium tungstate were obtained by applying conveniently chosen deformations to the original cubic lattice and fitting the resulting dependence of the total energy on the adimensional lattice strain parameter (see Fig. 2).[25] The atomic positions were fully relaxed each time the unit cell was deformed. Instead of calculating c_{12} directly from a convenient lattice distortion (which would reduce symmetry, leading to a higher computational cost), this elastic constant was obtained from the bulk modulus (B) and c_{11} through (1). The α-ZrW_2O_8 bulk modulus was obtained by applying a isotropic strain deformation to the cubic lattice and fitting the corresponding energy dependence on the lattice strain.[25] Table V shows a summary of the calculated elastic constants along with experimental results obtained near 0 K.[24] The agreement between experimental and calculated elastic constants is very good.

An issue that has been the subject of controversy in the scientific literature concerns the compressibility of ZrO_6 and WO_4 polyhedra and also the relative stiffness of the Zr-O-W linkage in the α-ZrW_2O_8 structure. Figure 3 shows the variation of some interatomic distances in zirconium tungstate as a function of pressure. Pressure was calculated from the unit cell volume using the Murnaghan equation of state
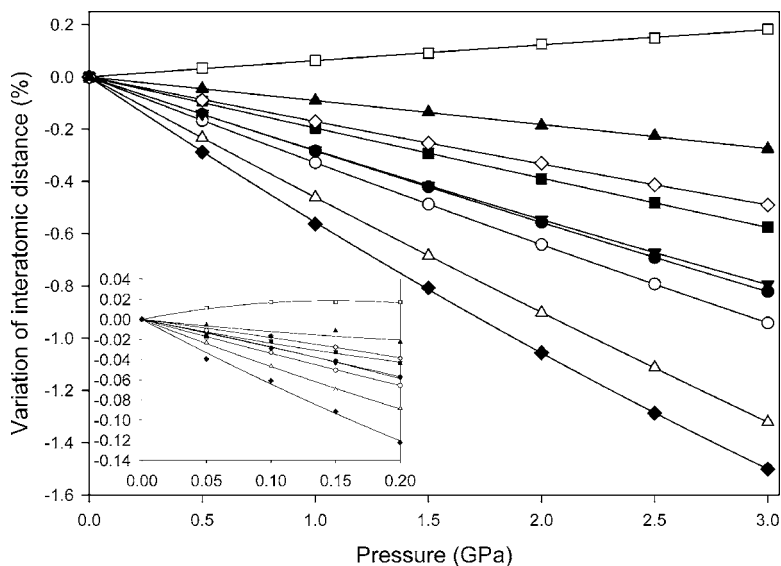
FIG. 3. Pressure dependence of some interatomic distances in α-ZrW$_2$O$_8$: Zr-W1 (●), Zr-W2 (○), Zr-O1 (▼), Zr-O2 (△), W1-O1 (■), W1-O3 (◆), W1-O4 (□), W2-O2 (◇), W2-O3 (▲). The solid lines are guides for the eye. The inset shows the same data over a narrow pressure range, up to 0.2 GPa.

(M-EOS).[34] The α-ZrW$_2$O$_8$ bulk modulus at zero pressure (B_0) and its pressure derivative B_0' [$B_0 = 100.2(6)$ GPa and $B_0' = 4.3(3)$], found by fitting the M-EOS to the energy-volume data, agrees very well with the bulk modulus calculated by imposing an isotropic strain to the cubic unit cell. As can be seen in Fig. 3 (see also Table VI), bond compressibilities varies from W1-O4 (whose bond length actually increases with pressure) to W1-O3 and Zr-O2, the more compressible bonds. Actually, despite bond valence calculations indicate that W1-O3 interaction contributes with approximately 5% of the total bonding around W1, these atoms hardly can be regarded as chemically bonded.[1] Overall, the relative stiffnesses of the atomic bonds (and linkages), ranked in terms of bond compressibilities, decrease according to the sequence W-O>Zr$\cdots$W>Zr-O. We will return to this issue in the discussion of the electronic density distribution in α-ZrW$_2$O$_8$.

The pressure dependence of the ZrO$_6$ and WO$_4$ polyhedral volume is shown in Fig. 4. Polyhedral volumes were calculated from the optimized atomic positions using the program IVTON.[36] The fitting of the Murnaghan equation of state to the data shown in Fig. 4 yields polyhedral bulk modulii at zero pressure of 87(1) GPa, 764(14) GPa, and 229(1) GPa for the octahedra around Zr and for the tetrahedra around W1 and W2, respectively. The numbers in parentheses represent the standard deviation of the fitted parameters. The fittings were performed keeping $B_0' = 4$. The tungsten polyhedra (and, particularly, that around W1) are thus much more stiff than the ZrO$_6$ octahedra, in accordance with the experimental results of Cao et al.[16,17] The larger bulk modulus for the tetrahedra around W1 results from the fact that the volume reduction upon pressure increase due to

the shortening of the W1-O1 bonds is partially compensated by the increase of the W1-O4 bond length. The W1-O4 bond length becomes larger with pressure probably as the result of the increasing W1-O3 interaction and the ensuing weakening of the W1-O4 bond. The inclusion of O3 in the coordination polyhedron around W1 reduces this polyhedron bulk modulus from 764(14) GPa to 129.5(2) GPa, lesser than that of the W2 polyhedra but still greater than the bulk modulus of the octahedra around Zr. This little exercise may help to put into perspective how much stiffer are the tungsten polyhedra in comparison with the ZrO$_6$ octahedra. It is noteworthy that the ZrO$_6$ polyhedral bulk modulus is actually lesser than that of the unit cell, a kind of inverted-molecular compressibility previously reported (and later disputed) for boron icosahedra in boron carbide.[37,38]

Table VII shows bond angles calculated for α-ZrW$_2$O$_8$ at zero pressure and their pressure derivatives. As can be seen, the Zr-O1-W1 and Zr-O2-W2 bond angle derivatives are very different. While the Zr-O2-W2 bond angle remains almost unchanged upon pressure increase, the Zr-O1-W1 linkage bends much more easily. Owing to the almost invariant Zr-O2-W2 bond angle, volume reduction with pressure proceeds through a more pronounced change of the Zr-O2 bond length, which is about 2 times more compressible than Zr-O1.

Despite the various W-O and Zr-O bond lengths and bond angles vary differently with pressure, overall the WO$_4$ and ZrO$_6$ polyhedra become slightly more regular upon increasing pressure. Indeed, in going from 0 GPa to 3 GPa, the M-O bond lengths decrease from 2.108 Å, 1.822 Å, and 1.806 Å to 2.085 Å, 1.815 Å, and 1.798 Å for Zr-O, W1-O, and W2-O, respectively. In the same pressure range, bond lengths' standard deviations are reduced from 0.045 Å,

TABLE VI. α-ZrW$_2$O$_8$ interatomic distances and bond compressibilities calculated at zero pressure.

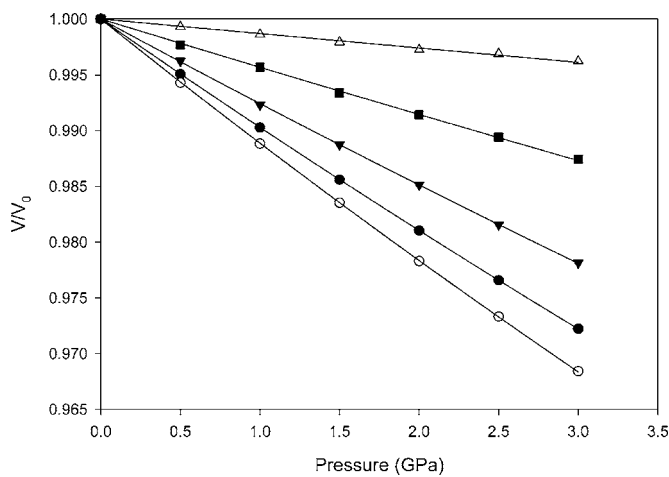| Atomic pair	Zr-W1	Zr-W2	Zr-O1	Zr-O2	W1-O1	W1-O4	W1-O3	W2-O2	W2-O3
Distance r(Å)	3.846	3.960	2.066	2.149	1.845	1.753	2.292	1.815	1.779
$d \ln r/dP$ ($\times 10^{-3}$ GPa^{-1})	-2.7	-3.5	-2.5	-4.9	-2.6	$+2.5$	-6.8	-1.7	-1.4

FIG. 4. The pressure dependence of polyhedral volume around W1 [$\triangle$ for the tetrahedra (W1,3O1,O4) and $\blacktriangledown$ for five-coordinated tungsten (W1,3O1,O4,O3)], W2 ($\blacksquare$), and Zr ($\bigcirc$). The pressure dependence of the unit cell volume ($\bullet$) is also shown for comparison. The solid curves represent the fittings of the Murnaghan equation of state to the data.

0.046 Å, and 0.018 Å to 0.039 Å, 0.040 Å, and 0.016 Å for Zr-O, W1-O, and W2-O, respectively. This conclusion, obtained from calculations on tetrahedrally coordinated tungsten, also holds for five-coordinated tungsten and also by considering a more restricted pressure range from 0 GPa to 0.2 GPa.

The observation that the WO_4 polyhedra are stiffer than the ZrO_6 octahedra is supported by the analysis of the electronic charge distribution in ZrW_2O_8, as it is shown in Fig. 5, where an equicharge density surface corresponding to 0.04 $e/\text{Å}^3$ is superimposed to a ball-and-stick representation of the α-ZrW_2O_8 crystal structure.[39] The equicharge density surface actually corresponds to the difference between the electronic charge distribution of the interacting atoms and that obtained from a simple superposition of atomic charge distributions. Hence, the isosurface depicted in Fig. 5 shows the rearrangement of the valence electron charge distribution resulting from bonding in zirconium tungstate. The charge envelope around the tungsten atoms, bridging them to the oxygen atoms, reveals the more pronounced covalent character of the W-O bonding. On the other hand, the absence of a charge build-up along the Zr-O bonds points to the predominantly ionic character of this bond, which makes it less stiff and contributes to the relatively low ZrO_6 polyhedral bulk modulus. The ionic character of the Zr-O bonding is in accordance with the conclusions from Drymiotis *et al.* whom, based on the Blackman diagram, have suggested a strong ionic contribution to interatomic bonding in zirconium tungstate.[24]
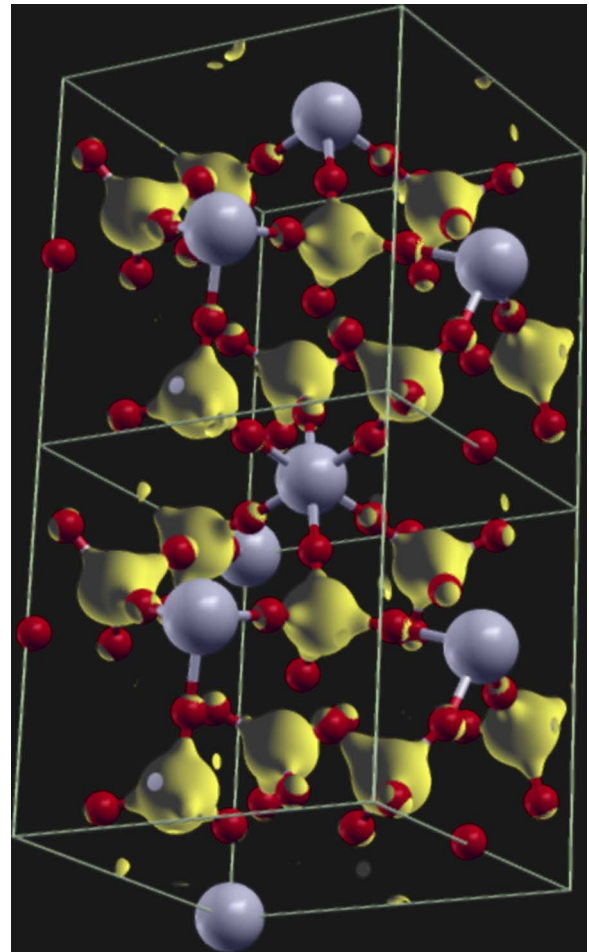

FIG. 5. (Color online) Charge-density difference isosurface drawn at 0.04 $e/\text{Å}^3$, obtained as the difference between the electronic charge distribution in α-ZrW_2O_8 and the pure superposition of atomic charge densities. For clarity the unit cell was duplicated along the *y* axis.

Figure 6 shows an equicharge density surface around W1 and W2 atoms, and reveals the stronger bonding between W1 and the terminal O4 atom, as expected from the shorter bond length. We have found no evidence of covalent bonding between W1 and W2 tetrahedra, as suggested by Kojima *et al.* from the analysis of powder diffraction data.[40]

Upon pressure increase the atoms tend to rearrange through a coordinated displacement along a pathway of minimum activation energy. Therefore, as far as the compression mechanism of zirconium tungstate could bear some resemblance to the low-energy modes responsible for the NTE in α-ZrW_2O_8, it is interesting to consider how the present results could contribute to clarify the controversy concerning the microscopic origin of this phenomenon. As
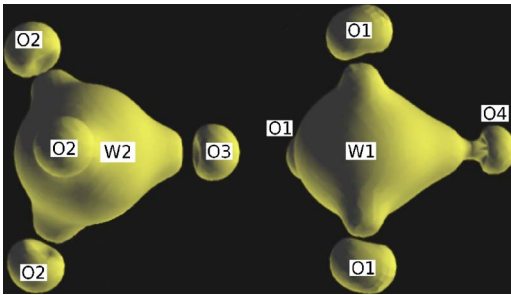
TABLE VII. Some bond angles calculated for α-ZrW_2O_8 at zero pressure. Bond angle pressure derivatives at zero pressure are given in parentheses, in units of 10^{-3} degrees GPa^{-1}.

Zr-O1-W1	Zr-O2-W2	O1-Zr-O1	O1-Zr-O2	O2-Zr-O2	O1-W1-O1	O1-W1-O4	O2-W2-O2	O2-W2-O3
159.1	175.0	91.78	86.50/89.93	92.82	118.2	97.73	110.2	108.7
(−236)	(−10)	(−126)	(+20)/(+78)	(+50)	(−82)	(+174)	(−98)	(+102)

FIG. 6. (Color online) Detail of the charge-density difference isosurface, drawn at $0.03 \, e/\text{Å}^3$ around the W1 and W2 atoms, showing the greater covalence of the shorter W1-O4 bond and the absence of any appreciable charge build up between W1 and O3.

mentioned before, based on the experimental observation that the Zr···W peaks in the Fourier transform of the α-ZrW$_2$O$_8$ XAFS spectra have a very small temperature dependence, Cao *et al.* have suggested that the Zr-O-W linkages are rigid and that NTE in zirconium tungstate is mainly caused by vibrational modes involving the correlated motion of a WO$_4$ tetrahedron and its three nearest ZrO$_6$ units.[16,17] On the other hand, reverse Monte Carlo analysis of neutron total scattering data led Tucker *et al.* to conclude that NTE in α-ZrW$_2$O$_8$ results from RUMs involving the correlated rotation of WO$_4$ and ZrO$_6$ polyhedra, which should behave as essentially rigid units.[19] Furthermore, according to Tucker *et al.*, a rigid Zr-O-W linkage would have the effect of stiffening the structure, inhibiting NTE in zirconium tungstate. Three points are of utmost importance in order to evaluate these two models for NTE in α-ZrW$_2$O$_8$ against our DFT results: (i) The relative stiffness of the ZrO$_6$ and WO$_4$ polyhedra, (ii) the rigidity of the Zr-O-W linkage, and (iii) the translational motion of the WO$_4$ units and the correlated motion of the three nearest ZrO$_6$ octahedra.

Concerning the relative stiffness of the ZrO$_6$ and WO$_4$ units, as we already have seen, the tungsten polyhedra are by far the most incompressible. The greater compressibility of the ZrO$_6$ octahedra can be traced back, in part, to the greater ionicity of the Zr-O bond (as compared to the W-O bond). The ZrO$_6$ octahedra are even more compressible than the α-ZrW$_2$O$_8$ unit cell, making it difficult to fit them into the rigid unit mode model. In fact, the Zr···W linkage is at least as rigid as the Zr-O bonds (the Zr-O2 bond, in particular, is far more compressible than the Zr···W1 and Zr···W2 linkages).

The issue about the bending of the Zr-O-W bond angle is more complex. As can be seen in Table VII, the pressure derivatives of the Zr-O1-W1 and Zr-O2-W2 bond angles are very different. While the former is easily bent (as required by the rigid unit mode model for NTE in zirconium tungstate), the latter is the hardest and agrees with the tent model of Cao *et al.* This observation has an impact on the third issue raised above. Upon pressure increase, as the Zr-O1-W1 bond bends, the distance between W1 and the plane formed by the

three nearest zirconium atoms diminishes. On the other hand, as pressure increases the distance between W2 and the plane formed by the three nearest zirconium atoms increases, while the Zr-O2-W2 bond angle remains almost unchanged.[41] The compression mechanism of the local structure around W2 thus resembles very well the tent model of Cao *et al.*, while the local structure around W1 accomodates the volume reduction mainly by correlated polyhedral rotation. The atomic displacement of the O2 atoms (bonded to W2), in particular, is about 2 times that of the O1 atoms (bonded to W1). Hence it may be possible that the recent controversy about the microscopic mechanism behind NTE in α-ZrW$_2$O$_8$ have arisen (at least in part) because both XAFS and total neutron scattering data only provide information about the average local structure around tungsten atoms, without making any distinction between W1 and W2 which, as we have seen, behaves very differently.

Summing up, as far as the α-ZrW$_2$O$_8$ compression mechanism could be related to the low-energy modes responsible for the NTE in this compound, we have found elements from both RUMs and tent models in our results. However, the relatively high compressibility of the ZrO$_6$ octahedra and the rigidity of the Zr-O2-W2 linkage hardly fit into the RUM model. Actually, the high compressibility of the ZrO$_6$ octahedra may be the reason why the relatively rigid Zr-O2-W2 linkage does not inhibit NTE in zirconium tungstate.

IV. CONCLUSION

The equilibrium structure, elastic constants and compression mechanism of α-ZrW$_2$O$_8$ were studied by means of B3LYP density functional theory calculations. Excellent agreement was found between calculated elastic constants and the recently reported experimental values for α-ZrW$_2$O$_8$ near 0 K. The compression mechanism of the local structure around W1 and W2 is different, and the ZrO$_6$ octahedra were shown to be more compressible than the WO$_4$ tetrahedra. In fact, the former are even more compressible than the α-ZrW$_2$O$_8$ unit cell. The greater Zr-O bond compressibility can be traced back to the greater ionicity of this bond. Some elements from the tent model and the rigid unit mode model for NTE in zirconium tungstate were found in the way the structure of this compound evolves upon increasing pressure. As far as the compression mechanism of α-ZrW$_2$O$_8$ can provide a path of volume reduction with minimum activation energy, the results presented in this paper could provide some insight on the low-energy modes responsible for NTE in zirconium tungstate.

*Electronic address: caperott@ucs.br

[1] T. A. Mary, J. S. O. Evans, T. Vogt, and A. W. Sleight, Science **272**, 90 (1996).

[2] J. Graham, A. D. Wadsley, J. H. Weymouth, and L. S. Williams, J. Am. Ceram. Soc. **42**, 570 (1959).

[3] C. Martinek and F. A. Hummel, J. Am. Ceram. Soc. **51**, 227 (1968).

[4] J. S. O. Evans, Z. Hu, J. D. Jorgensen, D. N. Argyriou, S. Short, and A. W. Sleight, Science **275**, 61 (1997).

[5] M. Auray and M. Quarton, Acta Crystallogr., Sect. C: Cryst. Struct. Commun. **51**, 2210 (1995).

[6] L. L. Y. Chang, M. G. Scroger, and B. Phillips, J. Am. Ceram. Soc. **50**, 211 (1967).

[7] J. D. Jorgensen, Z. Hu, S. Teslic, D. N. Argyriou, S. Short, J. S. O. Evans, and A. W. Sleight, Phys. Rev. B **59**, 215 (1999).

[8] J. S. O. Evans, J. D. Jorgensen, S. Short, W. I. F. David, R. M. Ibberson, and A. W. Sleight, Phys. Rev. B **60**, 14643 (1999).

[9] C. A. Perottoni and J. A. H. da Jornada, Science **280**, 886 (1998).

[10] A. S. Pereira, C. A. Perottoni, and J. A. H. da Jornada, J. Raman Spectrosc. **34**, 578 (2003).

[11] C. A. Perottoni, J. E. Zorzi, and J. A. H. da Jornada, Solid State Commun. **134**, 319 (2005).

[12] A. W. Sleight, Annu. Rev. Mater. Sci. **28**, 29 (1998).

[13] A. K. A. Pryde, K. D. Hammonds, M. T. Dove, V. Heine, J. D. Gale, and M. C. Warren, J. Phys.: Condens. Matter **8**, 10973 (1996).

[14] G. Ernst, C. Broholm, G. R. Kowach, and A. P. Ramirez, Nature (London) **396**, 147 (1998).

[15] A. P. Ramirez and G. R. Kowach, Phys. Rev. Lett. **80**, 4903 (1998).

[16] D. Cao, F. Bridges, G. R. Kowach, and A. P. Ramirez, Phys. Rev. Lett. **89**, 215902 (2002).

[17] D. Cao, F. Bridges, G. R. Kowach, and A. P. Ramirez, Phys. Rev. B **68**, 014303 (2003).

[18] J. N. Hancock, C. Turpen, Z. Schlesinger, G. R. Kowach, and A. P. Ramirez, Phys. Rev. Lett. **93**, 225501 (2004).

[19] M. G. Tucker, A. L. Goodwin, M. T. Dove, D. A. Keen, S. A. Wells, and J. S. O. Evans, Phys. Rev. Lett. **95**, 255501 (2005).

[20] A. K. A. Pryde, M. T. Dove, and V. Heine, J. Phys.: Condens. Matter **10**, 8417 (1998).

[21] R. Mittal and S. L. Chaplot, Phys. Rev. B **60**, 7234 (1999).

[22] N. L. Allan, G. D. Barrera, J. A. Purton, C. E. Sims, and M. B. Taylor, Phys. Chem. Chem. Phys. **2**, 1099 (2000).

[23] L. Ouyang, Y. N. Xu, and W. Y. Ching, Phys. Rev. B **65**, 113110 (2002).

[24] F. R. Drymiotis, H. Ledbetter, J. B. Betts, T. Kimura, J. C. Lashley, A. Migliori, A. P. Ramirez, G. R. Kowach, and J. VanDuijn, Phys. Rev. Lett. **93**, 025502 (2004).

[25] V. R. Saunders, R. Dovesi, C. Roetti, R. Orlando, C. M. Zicovich-Wilson, N. M. Harrison, K. Doll, B. Civalleri, I. Bush, Ph. D'Arco, and M. Llunell, *CRYSTAL2003 User's Manual* (University of Torino, Torino, 2003).

[26] A. D. Becke, J. Chem. Phys. **98**, 5648 (1993).

[27] R. Dovesi, C. Roetti, C. Freyria-Fava, M. Prencipe, and V. R. Saunders, Chem. Phys. **156**, 11 (1991).

[28] R. Dovesi and S. Gennard, http://www.crystal.unito.it/Basis_Sets/zirconium.html.

[29] D. Andrae, U. Häußermann, M. Dolg, H. Stoll, and H. Preuß, Theor. Chim. Acta **77**, 123 (1990); see also www.theochem.uni-stuttgart.de.

[30] H. J. Monkhorst and J. D. Pack, Phys. Rev. B **13**, 5188 (1976).

[31] G. Gilat and J. L. Raubenheimer, Phys. Rev. **144**, 390 (1966).

[32] H. B. Schlegel, J. Comput. Chem. **3**, 214 (1982).

[33] J. S. O. Evans, W. I. F. David, and A. W. Sleight, Acta Crystallogr., Sect. B: Struct. Sci. **55**, 333 (1999).

[34] F. D. Murnaghan, Proc. Natl. Acad. Sci. U.S.A. **30**, 244 (1944).

[35] A. Zupan and M. Causà, Int. J. Quantum Chem. **56**, 337 (1995).

[36] T. Balic Zunic and I. Vickovic, J. Appl. Crystallogr. **29**, 305 (1996).

[37] R. J. Nelmes, J. S. Loveday, R. M. Wilson, W. G. Marshall, J. M. Besson, S. Klotz, G. Hamel, T. L. Aselage, and S. Hull, Phys. Rev. Lett. **74**, 2268 (1995).

[38] N. Vast, J. M. Besson, S. Baroni, and A. Dal Corso, Comput. Mater. Sci. **17**, 127 (2000).

[39] A. Kokalj, Comput. Mater. Sci. **28**, 155 (2003); code available at www.xcrysden.org/.

[40] A. Kojima, Y. Kuroiwa, S. Aoyagi, A. Sawada, Y. Yamamura, N. Nakajima, and T. Tsuji, J. Korean Phys. Soc. **42**, S1257 (2003).

[41] A computer animation of the α-ZrW$_2$O$_8$ compression mechanism can be found at www.ucs.br/ccet/defq/caperott/zrw2o8.html.